Supporting Information

Selective CO Production by Photoelectrochemical Methane Oxidation on TiO_2

Wei Li[1,‡], Da He[1,‡], Guoxiang Hu[2], Xiang Li[1], Gourab Banerjee[3], Jingyi Li[1], Shin Hee Lee[3], Qi Dong[1], Tianyue Gao[1], Gary W. Brudvig[3], Matthias M. Waegele[1], De-en Jiang[2], and Dunwei Wang[1,*]

1. Department of Chemistry, Merkert Chemistry Center, Boston College, Chestnut Hill, Massachusetts 02467, United States
2. Department of Chemistry, University of California, Riverside, California 92521, United States
3. Department of Chemistry and Yale Energy Sciences Institute, Yale University, New Haven, Connecticut 06520-8107, United States

‡ These authors contributed equally.

Direct correspondence to D. Wang, email: dunwei.wang@bc.edu, Tel: +1-617-552-3121

Table of Contents

Experimental details

Figure S1. Raman spectra of ALD TiO_2 (**Sample 1**), commercial anatase TiO_2 (**Sample 2**) and P25 (**Sample 3**).
Figure S2. Linear sweep voltammogram of ALD TiO_2 in N_2 or CH_4-saturated 1.0 M NaOH electrolyte.
Figure S3. Stability test of the photoelectrode.
Figure S4. Cyclic voltammogram of ALD TiO_2 in CH_4 or CO-saturated 1.0 M NaOH electrolyte.
Figure S5. Faradaic efficiency with error bars of CO and O_2 evolution from ALD TiO_2.
Figure S6. O 1s XPS spectra of (a) as-prepared ALD TiO_2 (b) ALD TiO_2 after PEC bulk electrolysis in the presence protection gas N_2 (c) ALD TiO_2 after PEC bulk electrolysis in the presence of CH_4.
Figure S7. ATR-FTIR spectra of ALD TiO_2 after PEC bulk electrolysis under N_2 or CH_4.
Figure S8. Dependence of the product selectivity on light intensity.
Figure S9. Product selectivity dependence on pH.
Figure S10. An alternative pathway from intermediate **2** to **8**.
Figure S11. Raman spectra of anatase TiO_2 without CD_4, with CD_4 under dark condition, and with CD_4 under illumination.
Figure S12. Linear sweep voltammogram of ALD TiO_2 under light or dark in CH_4-saturated 1.0 M KNO_3 electrolyte in the FTIR set-up.
Figure S13. FTIR spectra for up to 34 min after the illumination was started.
Figure S14. Gibbs free energy changes (ΔG) for both CO and carbonate pathways.

Schematic S1. Comparison of CH_4 under different conditions: w/light, w/electricity; w/light, w/o electricity; w/o light, w/o electricity; w/o light, w/electricity.
Schematic S2. Demonstration of the experimental set-up in *in situ* Raman measurement.
Schematic S3. Demonstration of the experimental set-up in *in operando* ATR-FTIR measurement.

Table S1. Comparison of carbonaceous products of ALD TiO_2 under different conditions.
Table S2. Faradaic efficiency of H_2 production on the cathode after PEC bulk electrolysis.
Table S3. The concentration of Ti^{3+} in ALD TiO_2 (**Sample 1**), commercial anatase TiO_2 (**Sample 2**) and P25 (**Sample 3**).
Table S4. Control experiments of H_2O_2 and CH_4 in 1 M NaOH under different experimental conditions.

References

Experimental details

Preparation of TiO_2 samples

ALD TiO_2: TiO_2 was deposited on a 2.2 mm thick glass slide coated with fluorine-doped tin oxide conductive film (7 Ω/sq surface resistivity, Sigma-Aldrich) in a Cambridge nanotech (Savannah 100) system as previously reported.[1] FTO coated glass substrate was cleaned in acetone, methanol, and deionized (DI) water. The reaction was performed at 275℃ with a constant flow of N_2 (UHP, 99.999%, Airgas) at 20 sccm (background pressure ~1000 mTorr). Ti(i-PrO)$_4$ (99.999% trace metals basis, Sigma-Aldrich) served as the Ti precursor, and was heated to 75℃. DI H_2O at room temperature was used as the oxygen precursor. The pulse and purge time for Ti(i-PrO)$_4$ and H_2O was 0.1s & 5s, and 0.01s & 10s, respectively. The dependence of photocurrent density on TiO_2 thickness was discussed in the application of solar water splitting, the optimum TiO_2 thickness was ~50 nm for planar devices corresponding with 3000 cycles growth. The ALD TiO_2 featured anatase (101) surface as previously reported.[1] Raman spectra confirmed the anatase phase of ALD TiO_2 (Figure S1), using an XploRA micro-Raman system (Horiba) with an excitation laser of 638 nm.

Commercial anatase TiO_2 and P25 TiO_2: Commercial anatase TiO_2 powder (Sigma Aldrich, 99.8% trace metal basis) or P25 TiO_2 powder (Evonik Industries, Aeroxide TiO_2 P25) was dispersed in ethanol to make a TiO_2 suspension solution with a concentration of 0.1 g/mL. The resulted solution was drop-casted on FTO substrate and followed a spin coating procedure at a rate of 2500 rpm. Then, the TiO_2 coated FTO substrate was annealed at 475℃ in air for 3 h to remove the solvents and improve the adhesion between FTO substrate and TiO_2.

Electrode fabrication: As-prepared TiO_2 samples were scratched to expose conductive FTO surface, and connected with a Cu wire using Ag paste (MG Chemicals, 8331 Silver Conductive Epoxy Adhesive) and protected with non-conductive epoxy (Loctites 615 Hysol Epoxy Adhesive) to leave an electrode surface area of ca. 1.0 cm^2.

Photoelectrochemical (PEC) characterizations

PEC characterizations were carried out using a potentiostat/galvanostat (CH Instruments CHI604C) at room temperature (20℃) unless otherwise noted. A three-electrode configuration was employed, with TiO_2 coated FTO substrate as the working electrode, SCE (CH instruments) as the reference electrode and a Pt wire as the counter electrode. The three electrodes were sealed in a three-neck flask (15 mL) by rubber stoppers (with all possible leaking parts protected by parafilm and high vacuum grease). 1.0 M NaOH (ACS reagent, > 97.0%, pellets, Sigma Aldrich) was used as electrolyte with a pH value of 13.6. The electrochemical cell was purged with the gas of interest (CH_4, N_2 or CO) to remove the dissolved O_2 in the electrolyte for at least 30 min prior to measurements and maintain 1 atm of the gas in the headspace during measurements. In a typical cyclic voltammetry or linear sweep voltammetry, the voltage was swept from cathodic to anodic direction at a rate of 20 $mV.s^{-1}$. The light source for all data presented in this work was a ultra-violet light source with 254 nm wavelength (UVGL-55 Handheld UV Lamp, P/N 95-0005-05, 6

Watt, UVP LLC.). Front-side illumination was applied for all measurements.

Products detection

CO detection: Similar to a typical PEC measurement, a three-electrode configuration was employed, except that CH_4 (UHP, 99.99%, Airgas) or N_2 (UHP, 99.999%, Airgas) gas was encapsulated during bulk electrolysis with coulometry. The evolved CO in the headspace was sampled with a gastight syringe (100 µL) for product analysis using GC-MS (Shimadzu QP2010 Ultra, with Carboxen 1010 PLOT column). CO (UHP, 99.9%, Airgas) was used to calibrate the GC-MS.

Carbonate detection: Measuring the weight increase of carbonate precipitation after bulk electrolysis was used to quantify the carbonate formed in electrolyte. Prior to experiments, DI water was boiled to remove dissolved CO_2. After bulk electrolysis of ALD TiO_2 photoelectrode in the presence of CH_4 was finished, 10.0 mL of 1.0 M $Ba(NO_3)_2$ (ACS, > 99%, Alfa Aesar) was added to the electrolyte (also to fresh electrolyte as controlled experiment). No significant difference was obtained, suggesting the amount of carbonate product in the electrolyte was beyond the detection limit by this method.

Carbonate adsorbed on the TiO_2 surface was characterized by X-ray photoelectron spectroscopy (XPS) and attenuated total reflection-Fourier transformed infrared spectroscopy (ATR-FTIR). XPS spectra in Figure S4 were obtained using K-alpha$^+$ XPS (Thermo Scientific, Al Kα = 1486.7 eV), showing the carbonate formation on ALD TiO_2 surface only after PEC bulk electrolysis in the presence of CH_4. ATR spectra in Figure S7 were obtained using a Brüker ATR model Alpha spectrometer with diamond as the ATR crystal. ALD TiO_2 with different electrolysis history was placed on ATR plate with elastic pressing to improve the contact between the sample and the crystal. Acetone was used to clean the ATR substrates between each measurement. Air spectrum was measured as background. Data were collected using the Omnic software package. Each spectrum was collected with 32 scans at a 2 cm^{-1} spectral resolution.

O_2 detection: The evolved O_2 by ALD TiO_2 was detected in situ using a Clark-type BOD oxygen electrode (Thermo Scientific 9708 DOP). For a typical experiment, the working electrode, the reference electrode, and the counter electrode were sealed in a three-neck flask by rubber stoppers (with all possible leaking parts covered by parafilm and high vacuum grease). CH_4 gas was purged in the electrolyte for at least 30 min and the headspace was protected by CH_4 gas to ensure an O_2 free environment. Once we removed the needle purging CH_4 gas into the electrolyte, and the oxygen sensor had been stabilized close to 0 ppm for a period time (5 min), the O_2 yield was read on a pH meter connected to the oxygen sensor.

H_2O_2 detection: After PEC electrolysis, 1 M HCl was used to adjust the pH of electrolyte to 2~2.5. Then 50 µL of the Mo catalyst was added into the solution and incubated for 3 min.[2] Finally, 0.5 mL starch solution with concentration of 2 wt% was added to the solution. If there was H_2O_2, the

solution would turn blue.

Calculations of efficiency and selectivity

The product efficiency refers to Faradaic efficiency defined as the ratio between the charge corresponding to the amount of product (CO or O_2) evolved and the total charge consumed during the reaction. Because carbonate was only observed on the surface of TiO_2 photoelectrode, its production efficiency was calculated by subtracting the efficiency of CO and O_2 from unity. The CO selectivity refers to the percentage of CO Faradaic efficiency among the total charges other than O_2 formation.

Since carbonate is subtracted from CO and O_2, we consider the error bar of the carbonate efficiency of not statistically significant. In the manuscript, we used the following equation for standard deviation calculations:

$$SD = \sqrt{\frac{\sum|x - \bar{x}|^2}{n}}$$

The calculated standard deviation represents the variation of our measurements on the product selectivity. From our calculations, we believe that our measurement is reasonably consistent and the trend of the data is reliable.

Spectroscopic measurements

EPR spectroscopy: A Bruker ELEXSYS E500 spectrometer equipped with a SHQ resonator was used for the EPR experiments. An Oxford ESR-900 continuous flow cryostat was used to measure spectra at 7.5 K. The EPR parameters used for recording the spectra are as follows: microwave frequency, 9.38 GHz; modulation frequency, 100 kHz; modulation amplitude, 19.95 G; microwave power, 5 mW; sweep time, 84 s; conversion time, 41 ms; time constant, 82 ms. Each spectrum was the average of two scans. Since the signal intensity is proportional to radical concentration, the quantity of Ti^{3+} was calculated and the results of three samples are listed in Table S3. The standard used was carefully weighed out 2,2-Diphenyl-1-picrylhydrazy (DPPH) standard (Analytical grade, Sigma Aldrich). The EPR spectrum of the standard was taken under identical conditions.

Raman spectroscopy: Raman spectra were obtained using a Horiba XploRA micro Raman system with excitation laser of 638 nm. Commercial anatase TiO_2 (Sigma Aldrich, 99.8% trace metal basis) was employed instead of ALD anatase TiO_2 film for more sufficient interaction with CH_4; 3% H_2O-saturated CH_4 was circulated and enclosed in a homemade quartz cell (Schematic S2). Spectra were collected under air, CH_4/H_2O and CD_4 (99 atom% D, Assay 99%, Sigma Aldrich)/H_2O with/without illumination by UV light respectively (the same light source in PEC characterizations).

ATR-FTIR spectroscopy: ATR-FTIR spectra were recorded using a Bruker Vertex 70 FTIR spectrometer (Billerica, MA) equipped with an MCT detector (FTIR-16; Infrared Associates;

Stuart, FL). The TiO_2 coated FTO glass slide was pressed on the ATR Si prism crystal and the configuration is depicted in Schematic S3. The preparation of the Si crystal followed the procedure reported previously.[3] Electrochemical experiments were carried out in a two-electrode configuration with a Pt foil (99.95%; BASi Inc.; West Lafayette, IN) as the reference/counter electrode. 0.10 M KNO_3 (99.999% trace metals basis, Sigma Aldrich) was used as the electrolyte at room temperature and it was purged for at least one hour by either N_2 (control experiment) or CH_4 before being added into the electrochemical cell. Figure S8 shows the linear sweep voltammogram (at a rate of 20 $mV \cdot s^{-1}$) of ALD TiO_2 under light illumination in CH_4-saturated 1.0 M KNO_3 electrolyte in the FTIR set-up. To ensure steady-state conditions, the target potential was held at 0.3 V vs. internal Pt. The applied potential 0.3 V vs. internal Pt in Figure 4b would correspond to 0.9 V vs. RHE in a 3-electrode configuration. The appearance of specific adsorbed intermediates on the electrode is highly sensitive to surface heterogeneity, applied potential, and the amount of dissolved CH_4. Pressing of the working electrode against the IR transparent prism results in an electrochemical cell configuration that brings about uncertainties in the applied potential and unfavorable mass-transport conditions. As a result, while the three bands reported in Figure 4 were observed in multiple experiments, they did not always appear concurrently and/or with the same magnitude (Figures 4 and S13).

Each reported spectrum was collected at a 2 cm^{-1} spectral resolution and a 40 kHz scanner velocity with 64 scans. The spectrum collected in the beginning of PEC bulk electrolysis was used as the reference, followed by the single beam spectrum collected at each corresponding time point. The change of optical density was calculated as follows,

$$\Delta\text{mOD} = -1000 \cdot \log(S_{\text{sample}}/S_{\text{reference}}).$$

Computational methods

Spin-polarized density functional theory (DFT) calculations were performed using the Vienna *ab initio* simulation package (VASP).[4] The on-site Coulomb interaction was included using the DFT+U method described by Dudarev *et al*.[5] in VASP with a Hubbard parameter U=3.5 eV for the Ti atoms. Electron exchange-correlation was represented by the functional of Perdew, Burke and Ernzerhof (PBE) of generalized gradient approximation (GGA).[6] The ion-electron interaction was described with the projector augmented wave (PAW) method.[7] A cutoff energy of 400 eV was used for the plane-wave basis set. The anatase TiO_2 (101) surface was modeled with a three-layer thick slab with a 3 × 1 super cell. A vacuum layer of 15 Å along the z-direction was employed. The Brillouin zone was sampled by (3×3×1) Monkhorst-Pack k-point mesh. The top two TiO_2 layers of the slab together with the adsorbates were allowed to relax and the convergence threshold for structural optimization was set to be 0.025 eV/Å in force. The van der Waals interactions were included using the DFT-D3 method.[8]

The change in Gibbs free energy (ΔG) for the reaction steps was defined as $\Delta G = \Delta E + \Delta E_{ZPE} - T\Delta S$. ΔE can be directly determined by the DFT total energies. ΔE_{ZPE} and ΔS are the zero-point energy difference and the entropy difference between the products and the reactants, respectively.

T is the temperature, and 298.15 K was used in the present work.

Safety comment

No unexpected or unusually high safety hazards were encountered.

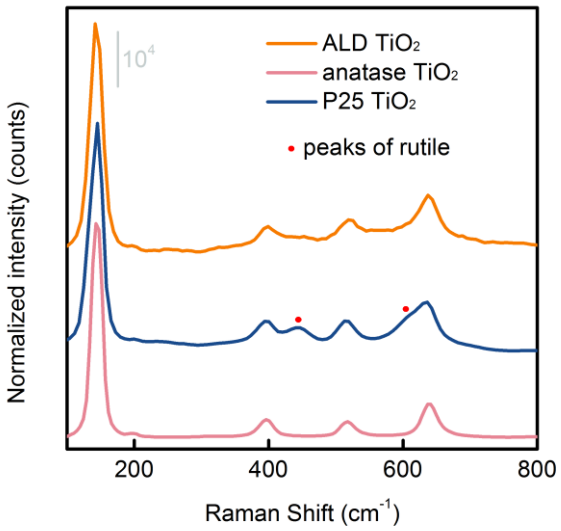

Figure S1. Raman spectra of ALD TiO_2 (**Sample 1**), commercial anatase TiO_2 (**Sample 2**) and P25 TiO_2 (**Sample 3**). Both **Sample 1** (orange trace) and **Sample 2** (pink trace) feature an anatase phase of TiO_2, **Sample 3** (blue trace) feature the mix phases of anatase and rutile of TiO_2.

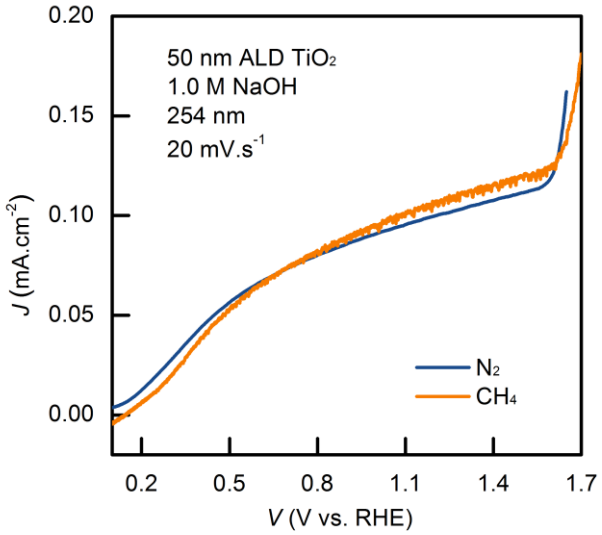

Figure S2. Linear sweep voltammogram of ALD TiO_2 in N_2 (blue trace) or CH_4 (orange trace)-saturated 1.0 M NaOH electrolyte at a rate of 20 $mV.s^{-1}$.

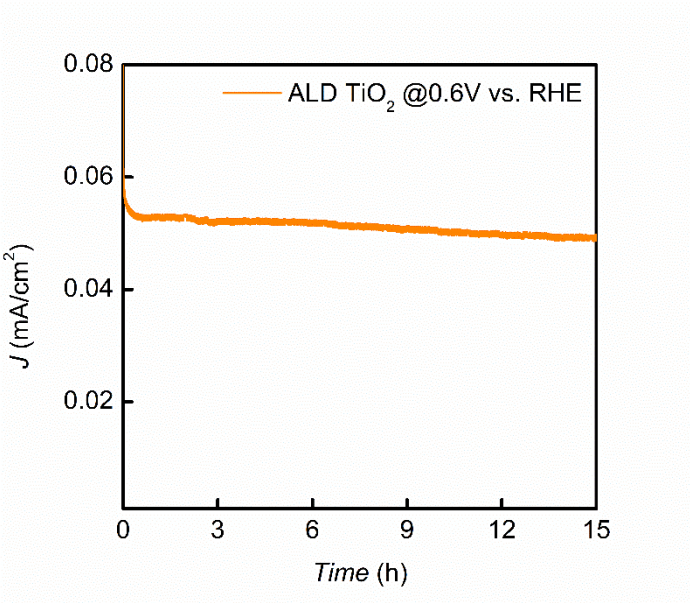

Figure S3. Stability test of the photoelectrode. Conditions: 0.6 V vs. RHE; UV illumination at 0.1 mW/cm^2.

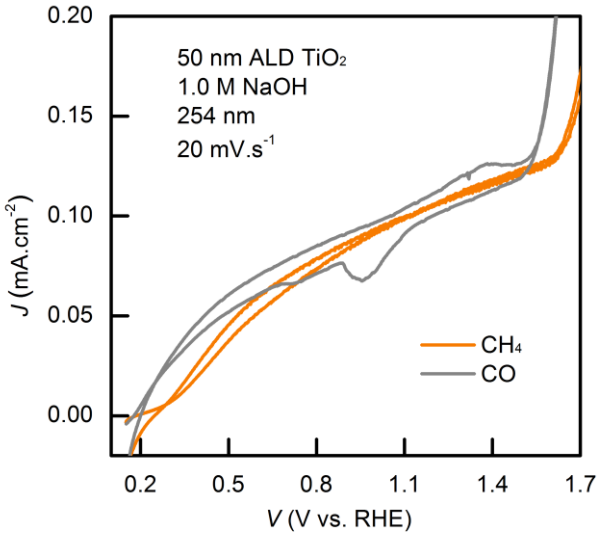

Figure S4. Cyclic voltammogram of ALD TiO_2 in CH_4 (orange trace) or CO (grey trace)-saturated 1.0 M NaOH electrolyte at a rate of 20 mV.s^{-1}.

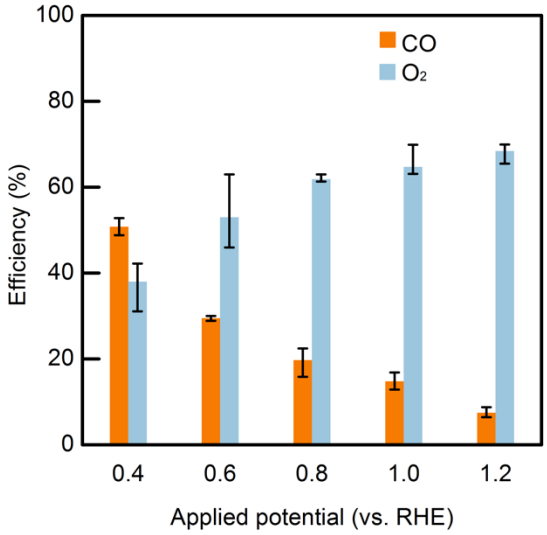

Figure S5. Faradaic efficiency with error bars of CO and O_2 evolution from ALD TiO_2. The applied potentials for PEC bulk electrolysis were hold from 0.4 V to 1.2 V vs. RHE with 200 mV intervals, in CH_4-saturated 1.0 M NaOH electrolyte.

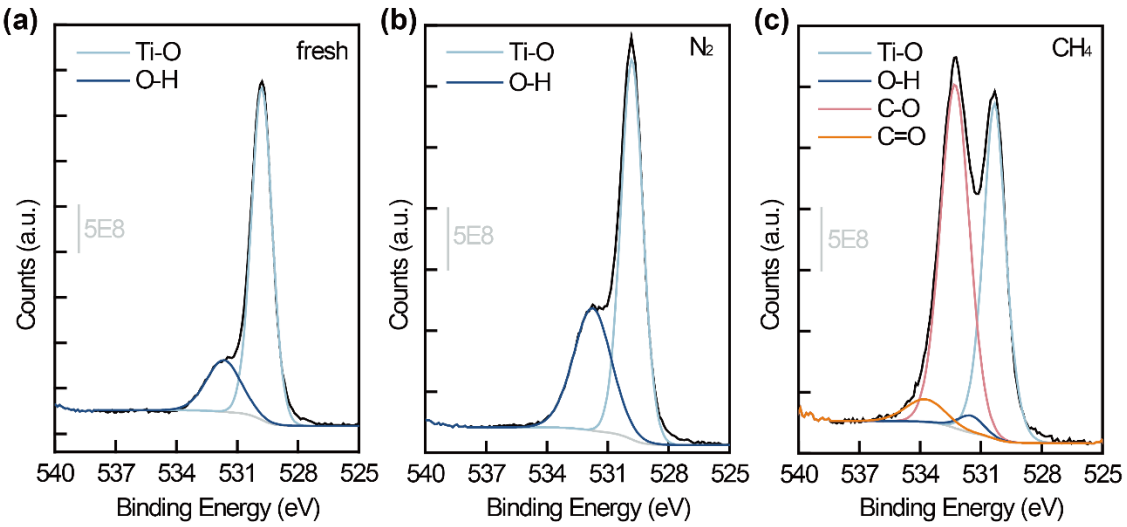

Figure S6. O 1s XPS spectra of (a) as-prepared ALD TiO_2 (b) ALD TiO_2 after PEC bulk electrolysis in the presence protection gas N_2 (c) ALD TiO_2 after PEC bulk electrolysis in the presence of CH_4.

In O 1s spectra shown (Figure S6a), as-prepared ALD TiO_2 photoelectrode shows two distinct features at 529.5 eV and 531.5 eV, representing lattice oxygen and surface hydroxyl groups, respectively. After PEC electrolysis under N_2, no significant difference was observed in Figure

S6b. By contrast, after PEC electrolysis under CH_4, new features arose at 532.2 eV and 533.5 eV in Figure S6c, which were ascribed to C-O and C=O formation.

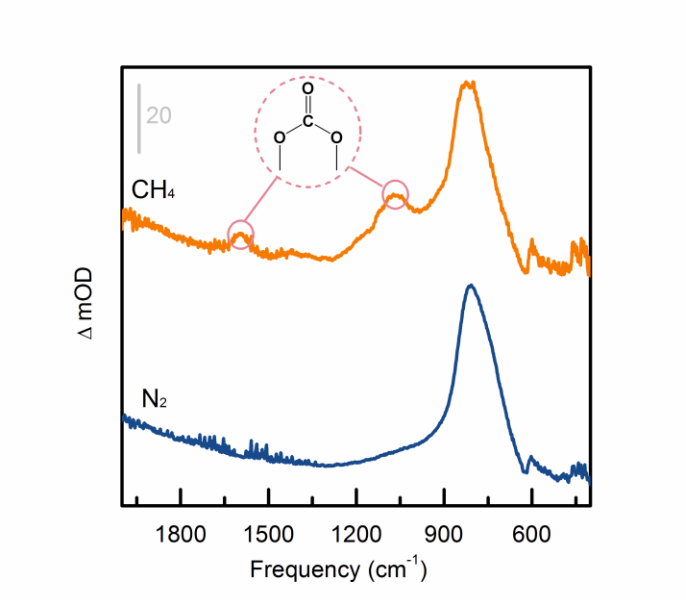

Figure S7. ATR-FTIR spectra of ALD TiO_2 after PEC bulk electrolysis under N_2 (blue trace) and CH_4 (orange trace). A diamond ATR crystal was employed in this experiment.

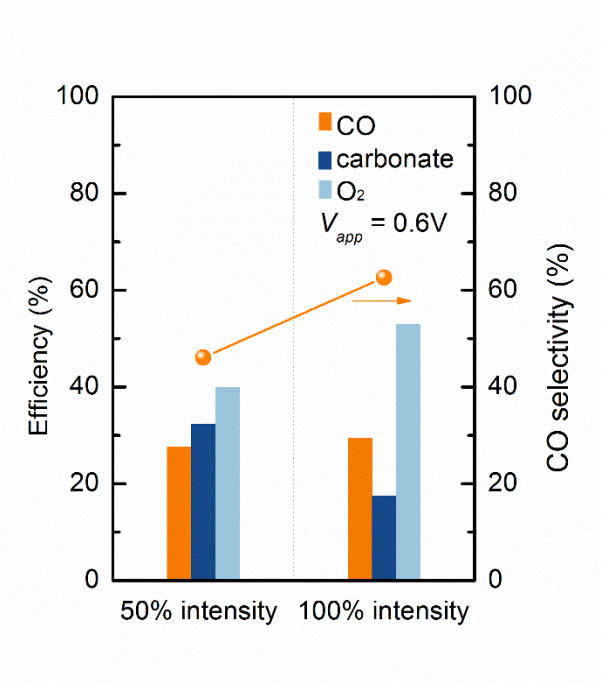

Figure S8. Dependence of the product selectivity on light intensity. Here 100% intensity refers to 0.1 mW/cm^2 at λ=254 nm.

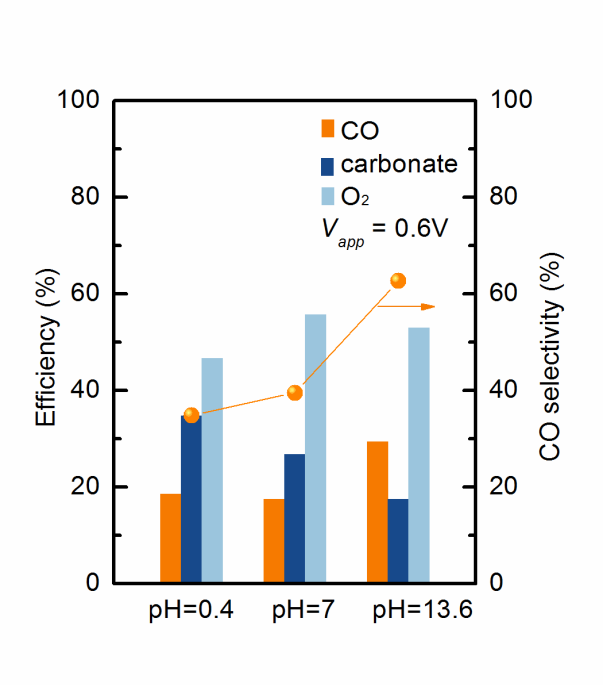

Figure S9. Product selectivity dependence on pH.

We carried out PEC bulk electrolysis (V_{app} = 0.6 V vs. RHE) in 0.5 M H_2SO_4 (pH = 0.4), 0.1 M KNO_3 (pH = 7) and 1.0 M NaOH (pH = 13.6), respectively. Higher CO_2 selectivity was observed at lower pH. This could be due to better CO_2 desorption as a gaseous product at lower pH. We were able to detect CO_2 by GC-MS at pH 0.4 in 0.5 M H_2SO_4 and observed quantitative correlation of the detected products (CO, CO_2 and O_2) with the measured charges.

The peak at 1073 cm^{-1} corresponds to the symmetric stretching mode of C=O in bidentate bicarbonate, and the peak at 1586 cm^{-1} corresponds to the asymmetric stretching mode of C=O in bidentate bicarbonate.[9]

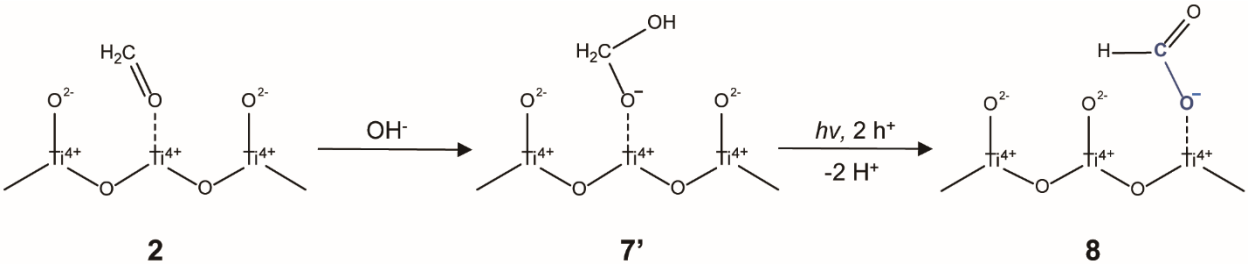

Figure S10. An alternative pathway from intermediate **2** to **8**. OH^- would undergo nucleophilic attack on the carbon atom of intermediate **2**, forming intermediate **7'**, which would undergo further

oxidation to **8** and finally to carbonate as the product.

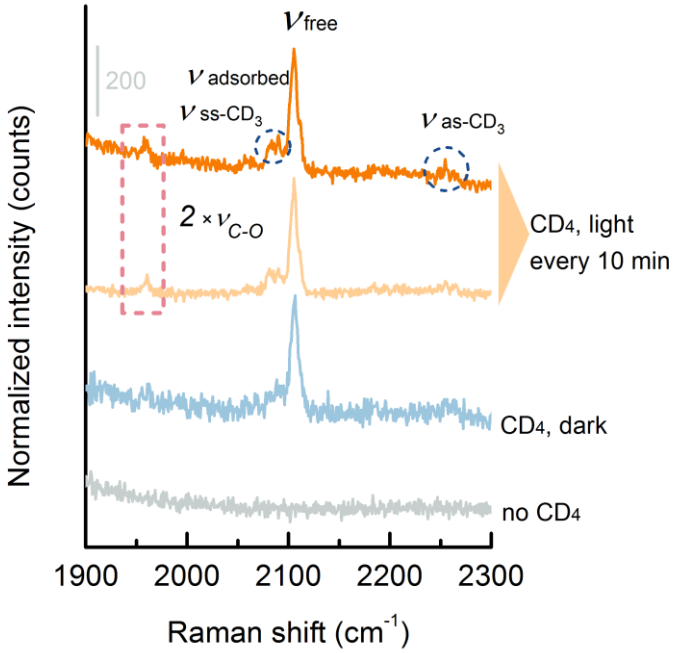

Figure S11. Raman spectra of anatase TiO_2 without CD_4, with CD_4 under dark condition, and with CD_4 under illumination.

Isotope-labelling (CD_4) measurements, with distinct targeted Raman shift region of C-D stretching modes (1800 cm^{-1} to 2500 cm^{-1}), are in excellent agreement with the above findings in CH_4. A manifest peak at 2101 cm^{-1} was attributed to free CD_4 molecule, and the emerging peaks under illumination at 2094, 2083 and 2250 cm^{-1} were assigned to adsorbed CD_4, symmetric stretching and asymmetric stretching mode in CD_3O, respectively.[10] Surprisingly, an additional peak was observed at 1974 cm^{-1} which is believed to represent the overtone of C-O stretching in CD_3O.[11] Taken together, the illumination-dependent peak evolution of surface-adsorbed CH_4 and CH_3O, and controlled isotope measurements validates our hypothesis that photoexcited TiO_2 at room temperature is active for C-H cleavage.

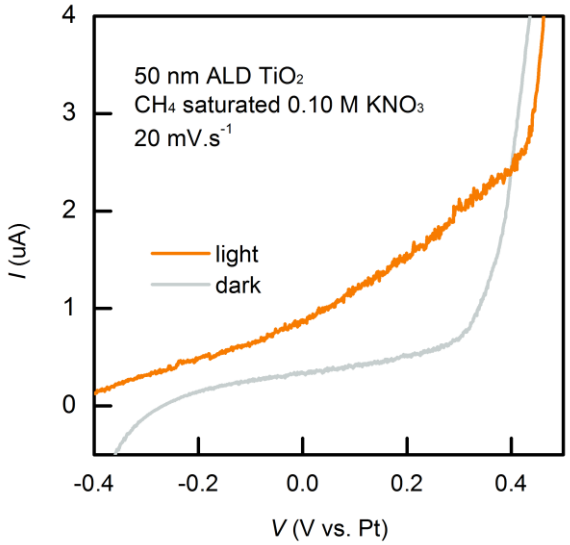

Figure S12. Linear sweep voltammogram (at a rate of 20 mV•s^{-1}) of ALD TiO_2 under light (orange trace) or dark (grey trace) in CH_4-saturated 1.0 M KNO_3 electrolyte in the FTIR set-up.

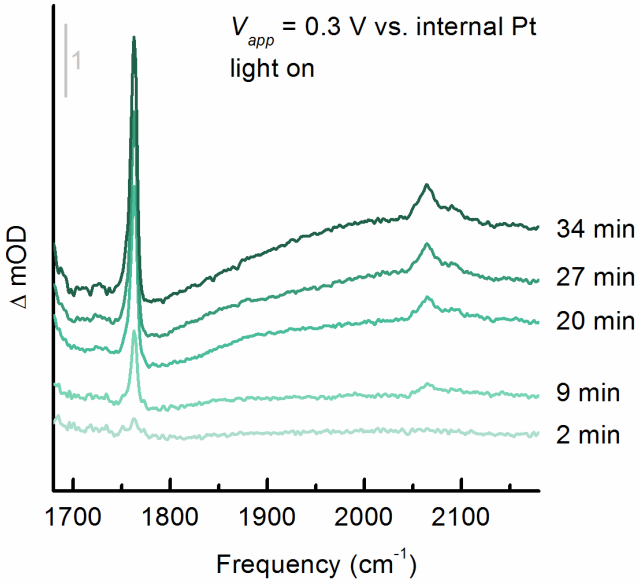

Figure S13. FTIR spectra for up to 34 min after the illumination was started.

The peaks at 1763 cm^{-1} and 2065 cm^{-1} were observed up to 34 min after the initiation of the reaction, and the observation was stopped at 34 min artificially.

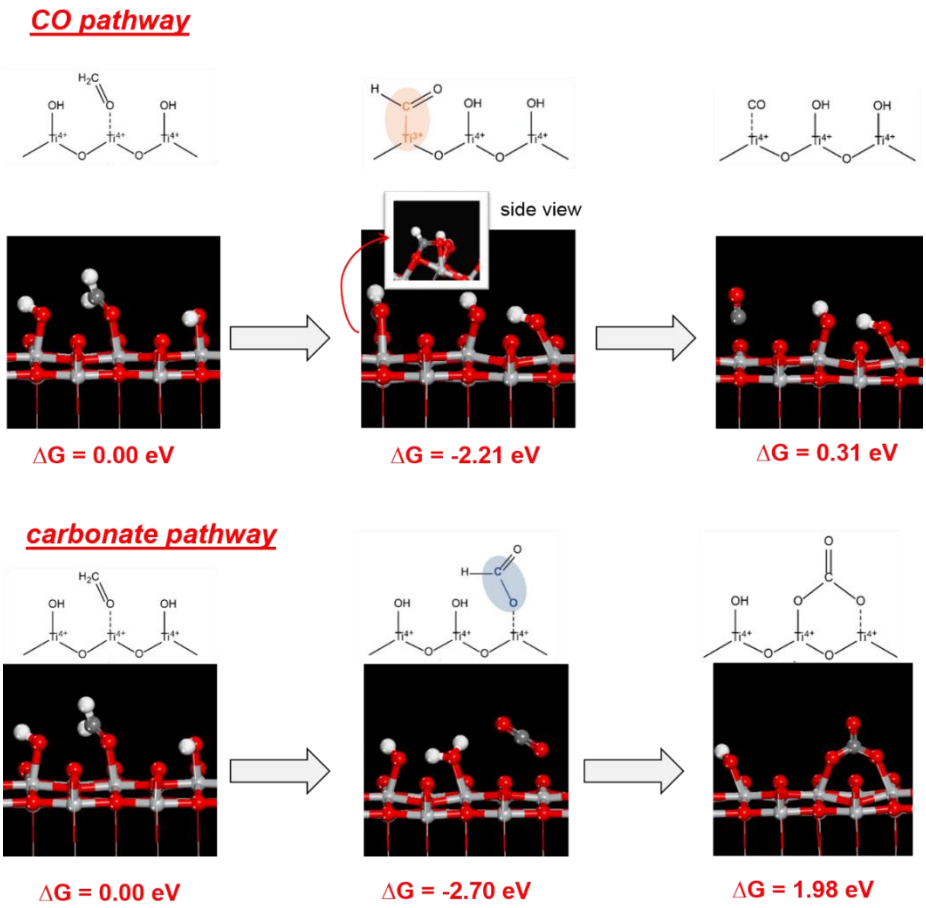

Figure S14. Gibbs free energy changes (ΔG) for both CO and carbonate pathways.

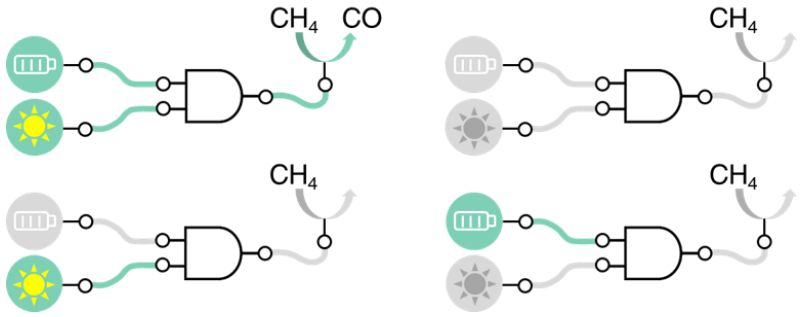

Scheme S1. CH_4 under different conditions: (top left) w/light, w/electricity; (bottom left) w/light, w/o electricity; (top right) w/o light, w/o electricity; (bottom right) w/o light, w/electricity.

No CO production was observed in any following scenario: only anodic applied potential (lack of radical species upon 254 nm light illumination on TiO_2); infrared light illumination (less sufficient to excite charges in TiO_2); no applied potential (less efficient excited charges separation in TiO_2) either in aqueous or gas phase.

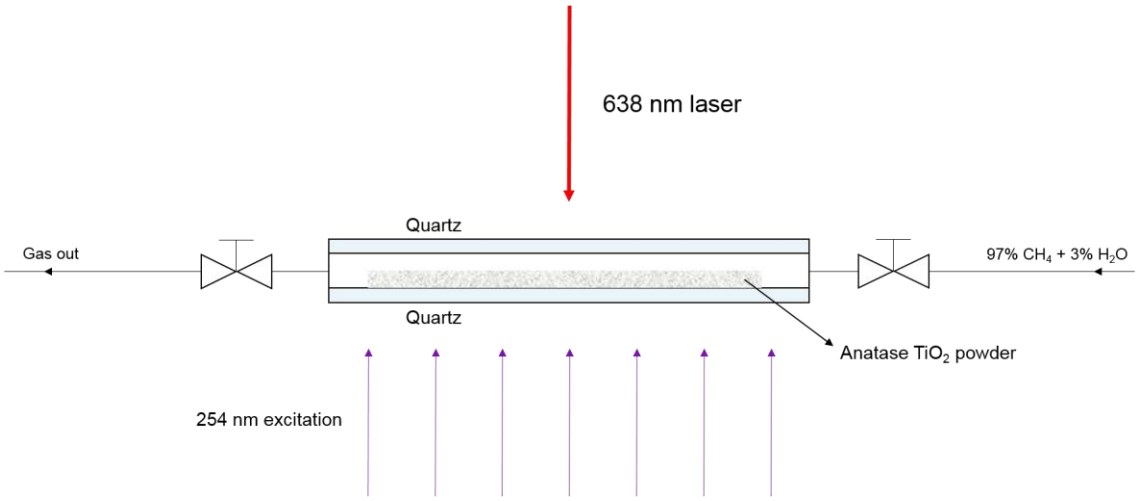

Scheme S2. Demonstration of the experimental set-up in *in situ* Raman measurement.

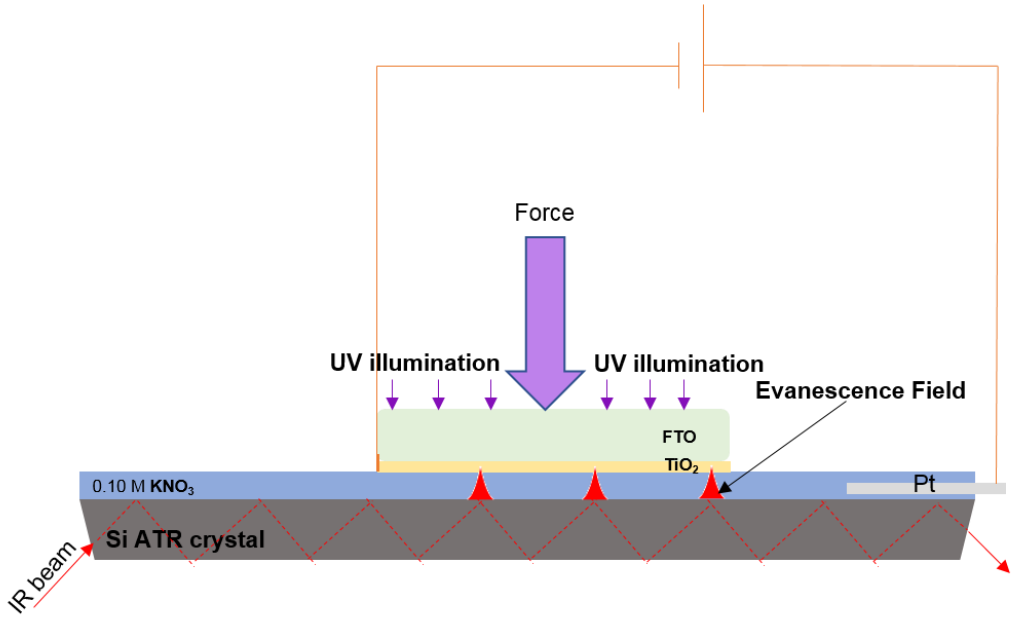

Scheme S3. Demonstration of the experimental set-up in *in operando* ATR-FTIR measurement.

Table S1. Comparison of carbonaceous products of ALD TiO_2 under different conditions.

Feed gas	E (vs. RHE)	Light	Carbonaceous Product	Faradaic efficiency
CH_4	0.4 V	254 nm	CO, carbonate	CO: 52.8 %
CH_4	1.7 V	off	--	--
CH_4	off	254 nm	--	--
CH_4	1.7 V	830 nm	--	--
N_2	0.4 V	254 nm	--	--

Table S2. H_2 production on the cathode accounts for ca. 100% Faradaic efficiency, ruling out the possibility that H_2 oxidation contributes to the measured photocurrent.

	Trail 1	Trail 2
Charge (**μmol**)	3.06	21.54
H_2 production (**μmol**)	1.51	9.85
FE (×100%)	98.9	91.5

Table S3. The concentration of Ti^{3+} in ALD TiO_2 (**Sample 1**), commercial anatase TiO_2 (**Sample 2**) and P25 (**Sample 3**).

	ALD TiO_2 **Sample 1**	Commercial anatase TiO_2 **Sample 2**	P25 **Sample 3**
Concentration of Ti^{3+}	32%	0.008%	0.08%

Table S4. Control experiments of H_2O_2 and CH_4 in 1 M NaOH under different experimental conditions.

Experimental conditions	CO (GC-MS)	Carbonate (FTIR)
TiO_2 w/light w/potential	No	No
TiO_2 w/light w/o potential	No	No

TiO_2 w/o light w/o potential	No	No
No TiO_2 w/ light w/o potential	No	No

The additional control experiments included: **1.** TiO_2 photoanode with H_2O_2 and CH_4 under illumination; **2.** TiO_2 photoanode with H_2O_2 and CH_4 without illumination; **3.** only H_2O_2 and CH_4 under illumination. None of these experiments yielded CO (as measured by GC-MS) or carbonates (as characterized by FTIR). These results prompted us to draw the following conclusions:

1. Under PEC conditions, H_2O_2 is likely oxidized more easily than CH_4. It implies that even if H_2O_2 (or other peroxide or superoxide) was indeed formed, it would likely be oxidized immediately before it could oxidize CH_4.
2. The results ruled out the possibility that CO production comes from the chemical reaction between H_2O_2 and CH_4.
3. The absence of CO or carbonate products suggests that CH_4 is unlikely to be activated by H_2O_2, under our reaction conditions, with or without light. This could be due to the ease of H_2O_2 oxidation by TiO_2. It could also be due to overoxidation of CH_4, as suggested by a reviewer.

Taken as a whole, we consider that CH_4 activation is unlikely due to the intermediates of H_2O oxidation.

References

(1) Lin, Y., Zhou, S., Liu, X., Sheehan, S.,Wang, D., TiO_2/$TiSi_2$ Heterostructures for High-Efficiency Photoelectrochemical H_2O Splitting. *J. Am. Chem. Soc.*, **2009**, *131*, 2772-2773.

(2) McCloskey, B. D., Valery, A., Luntz, A. C., Gowda, S. R., Wallraff, G. M., Garcia, J. M., Mori, T. and Krupp, L. E. Combining Accurate O_2 and Li_2O_2 Assays to Separate Discharge and Charge Stability Limitations in Nonaqueous Li–O_2 Batteries. *J. Phys. Chem. Lett.*, **2013**, *4*, 2989-2993.

(3) Gunathunge, C. M., Li, X., Li, J., Hicks, R. P., Ovalle, V. J.,Waegele, M. M., Spectroscopic Observation of Reversible Surface Reconstruction of Copper Electrodes under CO_2 Reduction. *J. Phys. Chem. C*, **2017**, *121*, 12337-12344.

(4) Kresse, G.,Furthmüller, J., Efficient Iterative Schemes for Ab Initio Total-Energy Calculations Using a Plane-Wave Basis Set. *Phys. Rev. B*, **1996**, *54*, 11169-11186.

(5) Dudarev, S. L., Botton, G. A., Savrasov, S. Y., Humphreys, C. J.,Sutton, A. P., Electron-Energy-Loss Spectra and the Structural Stability of Nickel Oxide: An Lsda+U Study. *Phys. Rev. B*, **1998**, *57*, 1505-1509.

(6) Perdew, J. P., Burke, K.,Ernzerhof, M., Generalized Gradient Approximation Made Simple. *Phys. Rev. Lett.*, **1996**, *77*, 3865-3868.

(7) Blöchl, P. E., Projector Augmented-Wave Method. *Phys. Rev. B*, **1994**, *50*, 17953-17979.

(8) Grimme, S., Antony, J., Ehrlich, S.,Krieg, H., A Consistent and Accurate Ab Initio Parametrization of Density Functional Dispersion Correction (DFT-D) for the 94 Elements H-Pu. *J. Chem. Phys.*, **2010**, *132*, 154104.

(9) Mino, L., Spoto, G.,Ferrari, A. M., CO_2 Capture by TiO_2 Anatase Surfaces: A Combined DFT and Ftir Study. *J. Phys. Chem. C*, **2014**, *118*, 25016-25026.

(10) Errahali, M., Gatti, G., Tei, L., Canti, L., Fraccarollo, A., Cossi, M.,Marchese, L., Understanding Methane Adsorption in Porous Aromatic Frameworks: An FTIR, Raman, and Theoretical Combined Study. *J. Phys. Chem. C*, **2014**, *118*, 10053-10060.

(11) Falk, M.,Whalley, E., Infrared Spectra of Methanol and Deuterated Methanols in Gas, Liquid, and Solid Phases. *J. Chem. Phys.*, **1961**, *34*, 1554-1568.